Electronic Supplementary Information

Crystal engineering in 3D: converting nanoscale lamellar manganese oxide to cubic spinel while affixed to a carbon architecture

Martin D. Donakowski,[a,b] Jean M. Wallace,[b,c] Megan B. Sassin,[b] Karena W. Chapman,[d] Joseph F. Parker,[b] Jeffery W. Long,[b] and Debra R. Rolison[b,*]

[a] *Postdoctoral Associate of the National Research Council (NRC), USA*
[b] *U. S. Naval Research Laboratory, Surface Chemistry Branch (Code 6170), Washington, D.C., 20375, USA. E-mail: rolison@nrl.navy.mil*
[c] *Nova Research, Inc., 1900 Elkin Street, Alexandria, VA 22308, USA*
[d] *X-ray Science Division, Advanced Photon Source, Argonne National Laboratory, Argonne, IL 60439, USA*

Table of Contents

Porosimetry

The surface area of the bare carbon nanofoam (CNF) was characterized with nitrogen physisorption (Micromeritics ASAP2020) to determine pore distributions for pores sized < 300 nm. The CNFs were cut with a fresh razor blade and degassed for 24 h at 150°C prior to characterization. The pore size distribution (Fig. S1) was calculated with Micromeritics ASAP2020 software using a density functional theory (DFT) model for a cylindrical geometry and Halsey curve thickness.

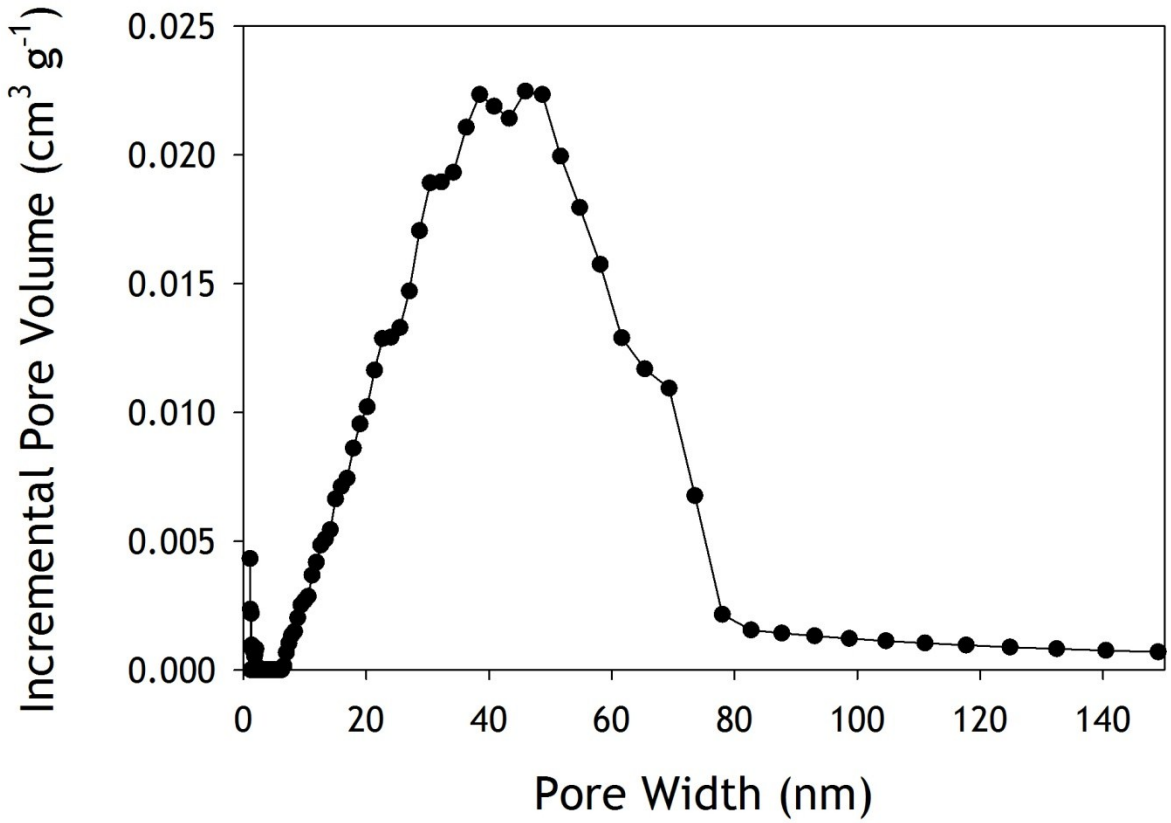

Fig. S1 Pore size distribution of unmodified carbon nanofoam (CNF).

Raman Spectroscopy

The Raman spectra were acquired as described in the main text. The D and G bands of the carbon peaks were fit with a summation, respectively, of a Lorentzian and Breit–Wigner–Fano (BWF) peak shape for the D and G bands. Peak intensities (I) were obtained from peak heights as previously described for disordered carbons. The BWF peak shape showed a coupling coefficient near zero indicating that the Raman band was localized and not coupled to a continuum. It was found that the data could not be fit to Gaussian functions but were fit to a summation of a Lorentzian term for the D band and a BWF term for the G band as previously described (equation S1).[1]

$$I(\omega) = Y_0 + \frac{Y_g[1 + \frac{2(\omega - \omega_g)}{Q\Gamma}]^2}{1 + \left[\frac{2(\omega - \omega_g)}{\Gamma}\right]^2} + \frac{Y_d}{1 + (\frac{\omega - \omega_d}{b})^2} \qquad \text{S1}$$

Wherein w is the wavenumber (cm^{-1}), I(w) is the observed intensity at w (arbitrary units), Y_0 is the baseline, Y_g is the intensity of the G band of the BWF peak, w_g is the center of the G band, Q^{-1} is the BWF coupling term, Γ is the full width at half maximum (FWHM), Y_d is the intensity of the D band, w_d is the center of the D band, and b is the FWHM.

In the case of the unmodified carbon nanofoam (CNF), an additional Gaussian term was added to account for an additional peak at lower energy than the D band:

$$I_{CNF}(\omega) = I(\omega) + \frac{a}{w_{ga}\sqrt{\frac{\pi}{2}}} * e^{\frac{-1}{2}\left(\frac{\omega - \omega_{ga}}{c}\right)^2} \qquad \text{S2}$$

wherein I(w) is derived from eqn S1, a is the area, w_{ga} is the peak center, and c is the FWHM. The results from the fits are shown in Figures S2–S10 and the parameters are tabulated in Table S1.

Raman Spectra Fits

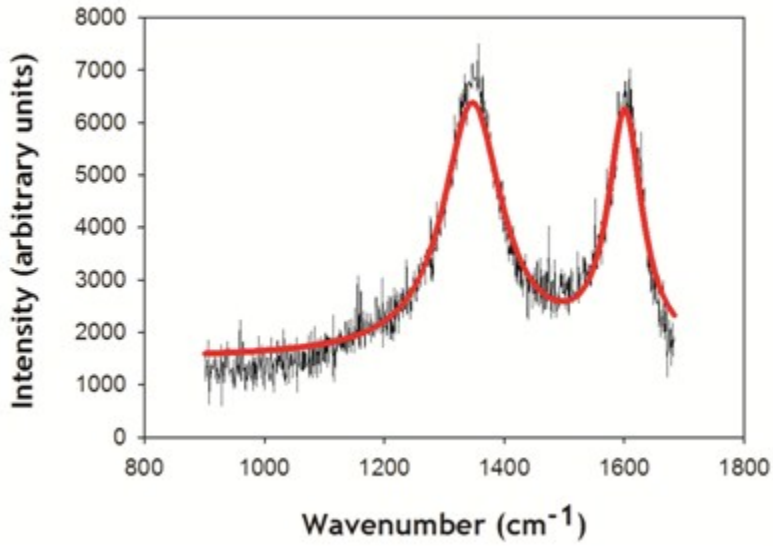

Fig. S2 Fit (—) of CNF (*i*) of D and G Raman bands to eqn. S1.

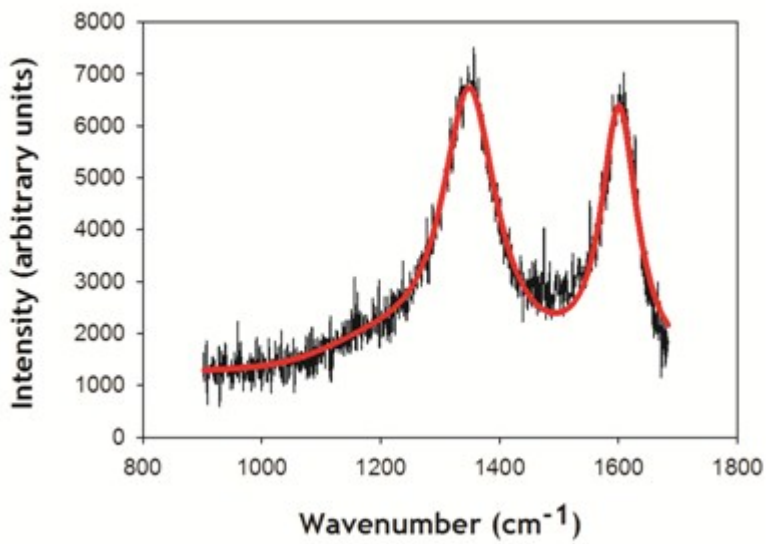

Fig. S3 Fit (—) of CNF (*i*) D and G Raman bands to eqn. S2.

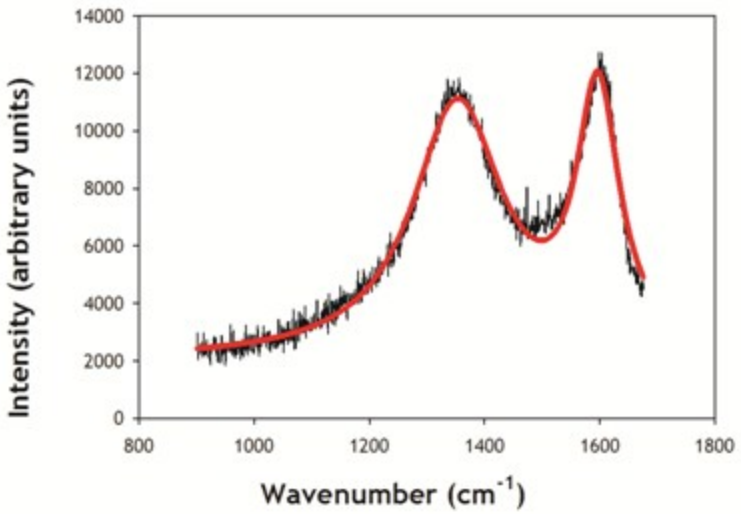

Fig. S4 Fit (—) of NaMnOx@CNF composite (*ii*) D and G Raman bands to eqn. S1.

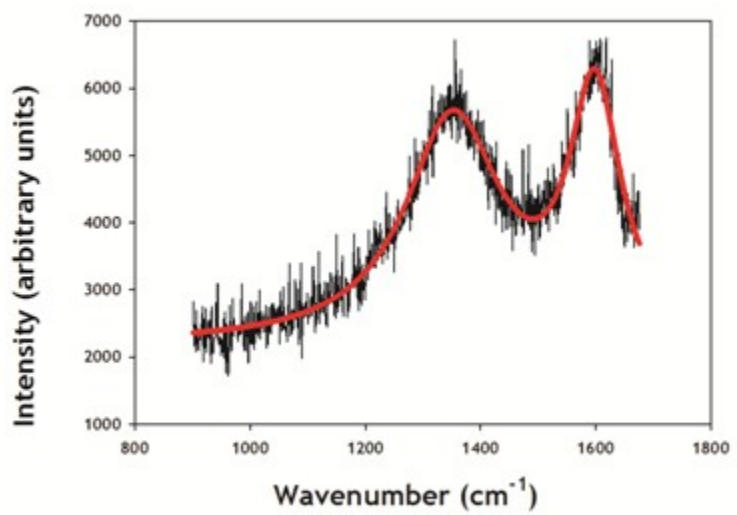

Fig. S5 Fit (—) of LiMnOx[8]@CNF composite (*iii*) D and G Raman bands to eqn. S1.

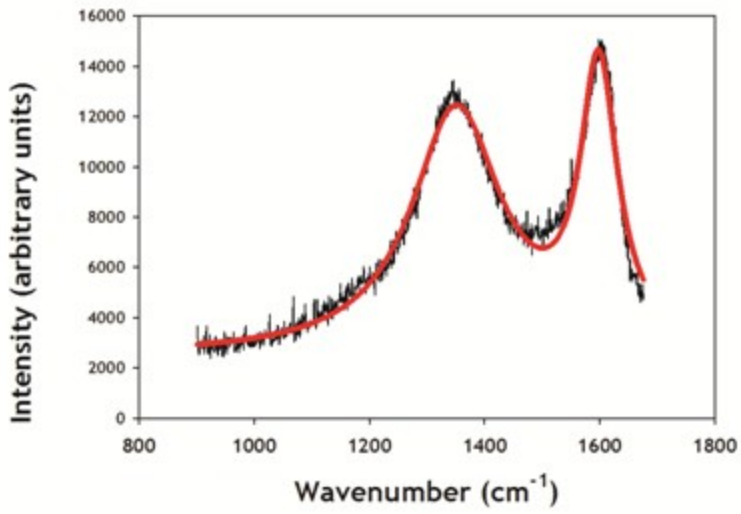

Fig. S6 Fit (—) of LiMnOx[24]@CNF composite (iv) D and G Raman bands to eqn. S1.

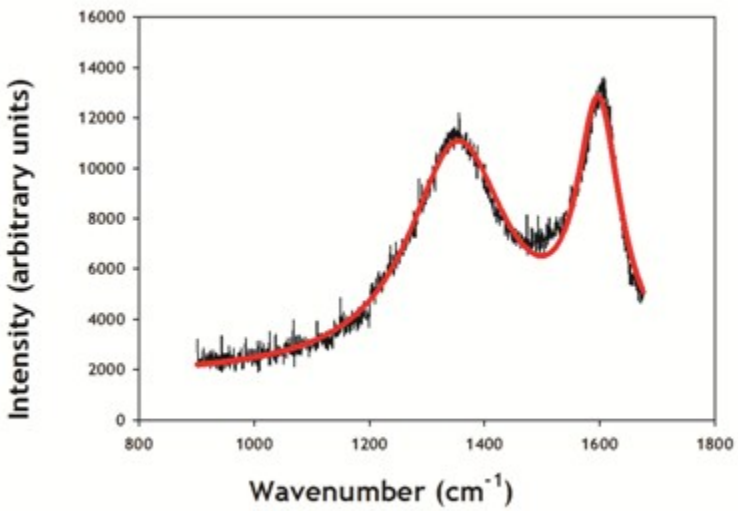

Fig. S7 Fit (—) of LiMnOx@CNF[Ar/1.33] composite (v) D and G Raman bands to eqn. S1.

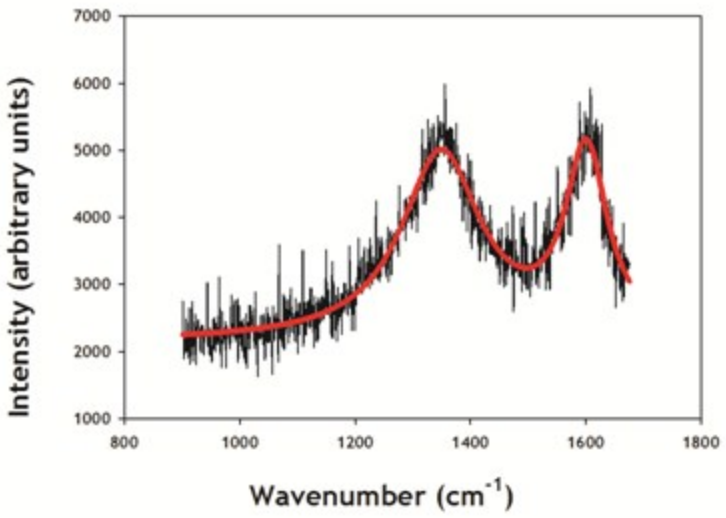

Fig. S8 Fit (—) of LiMnOx@CNF[Ar/4] composite (vi) D and G Raman bands to eqn S1.

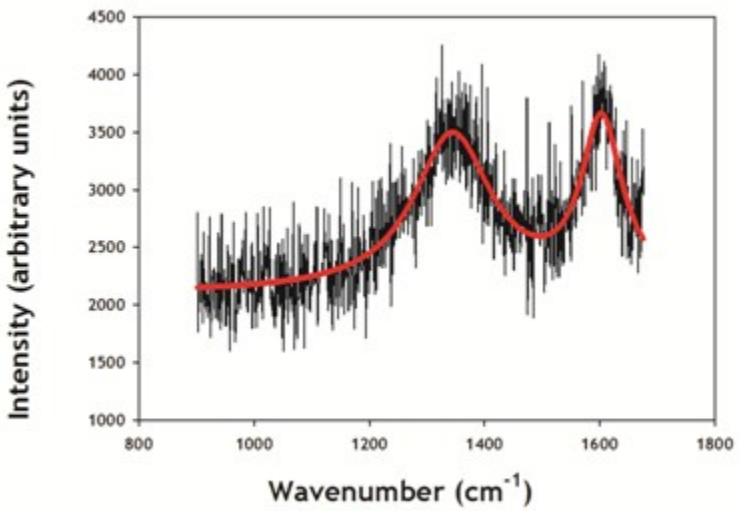

Fig. S9 Fit (—) of LiMnOx@CNF[Ar/4][Air/2] composite (vii) D and G Raman bands to eqn. S1.

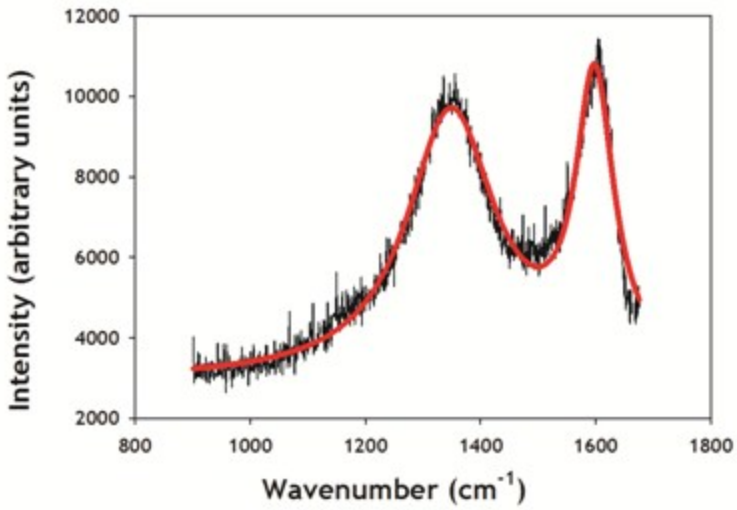

Fig. S10 Fit (—) of LiMnOx@CNF[Ar/4][Air/6] composite (*viii*) D and G Raman bands to eqn. S1.

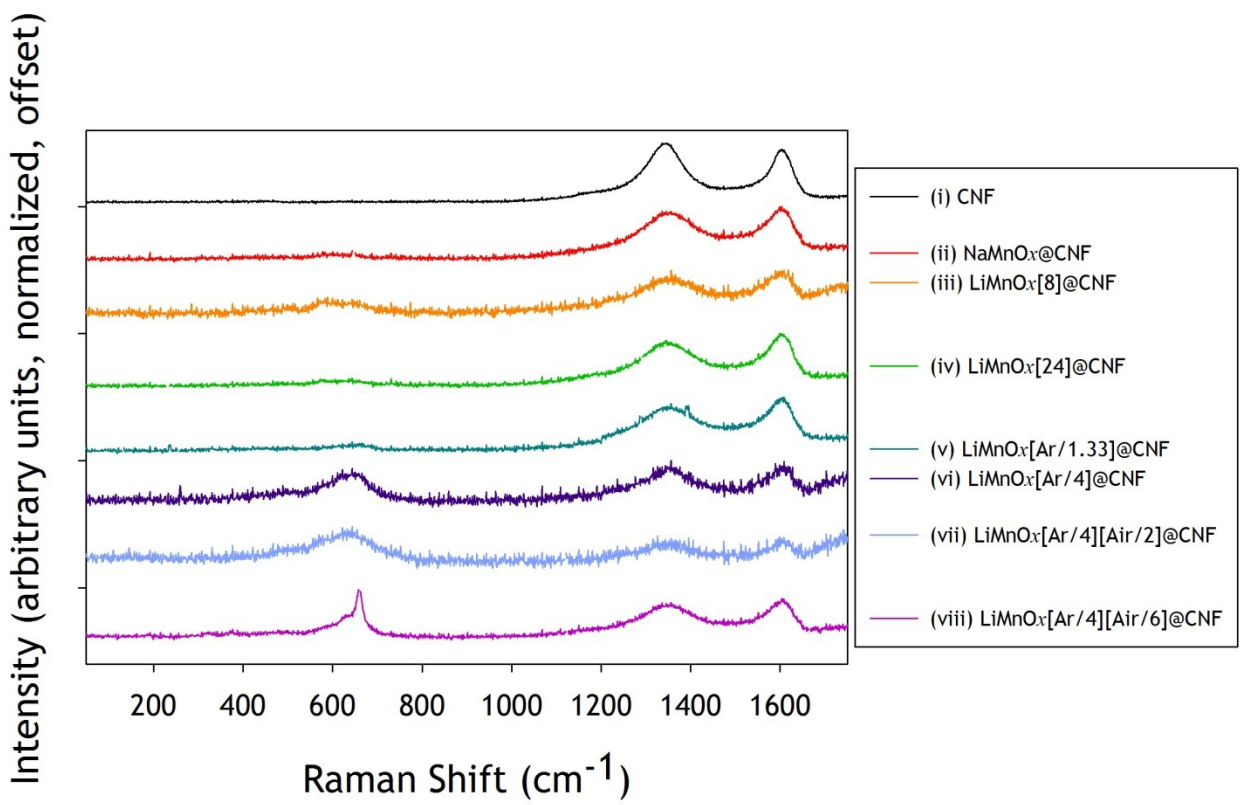

Fig. S11 The Raman spectra for composites (*i*)–(*viii*); the spectra are offset and normalized in intensity for clarity.

Raman Fit Parameters

Substrate:	CNF (*i*)	NaMnO*x*@CNF (*ii*)	LiMnO*x*[8]@CNF (*iii*)	LiMnO*x*[24]@CNF (*iv*)	LiMnO*x*[Ar/1.33]@CNF (*v*)	LiMnO*x*[Ar/4]@CNF (*vi*)	LiMnO*x*[Ar/4][Air/2]@CNF (*vii*)	LiMnO*x*[Ar/4][Air/6]@CNF (*viii*)
Y_0[a]	1198.6	2017.3	2180.6	2490.5	1693.6	2146.5	2101.9	2936.7
Y_d[a]	5364.1	8838.2	3333.6	9722.1	9084.7	2790.9	1364.9	6617.9
b[b]	1348.9	1352.8	1351.7	1350.8	1353.5	1348.7	1343.8	1348.6
w_d[b]	55.9	96.2	101.2	95.6	106.3	84.3	82.2	94.1
Y_g[a]	2473.1	4439.5	1817.5	5462.8	4869.8	1375.9	721.6	3532.3
w_g[b]	1600.8	1596.8	1598.4	1598.3	1597.8	1600.7	1603.5	1598.2
Q*	100.0	100.0	100.0	100.0	100.0	100.0	100.0	100.0
Γ[b]	72.8	89.4	108.6	78.2	91.2	89.2	86.2	80.2
a[c]	29856							
w_{gc}[b]	1195							
c[b]	60.7							

Table S1 Refinement parameters of Raman spectra to eqns S1 and S2.

* Constrained Q to values ≤ 100.

XPS Spectra

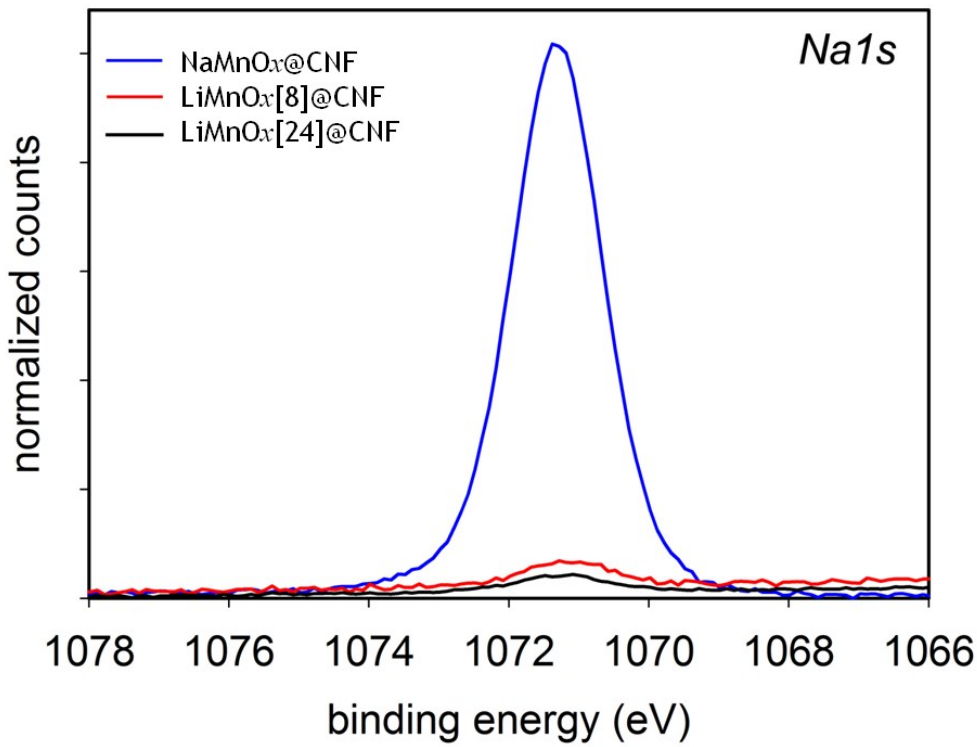

Fig. S12 XPS spectra in the Na1s region. The peak intensity for the Na1s line for each composite is normalized relative to the intensity of its C1s peak at 284.6 eV; a decrease in Na^+ content is observed in composites LiMnOx[8]@CNF (*iii*) and LiMnOx[24]@CNF (*iv*) after soaking NaMnOx@CNF (*ii*) in an aqueous 1 M $LiNO_3$ solution.

Powder X-ray Diffraction

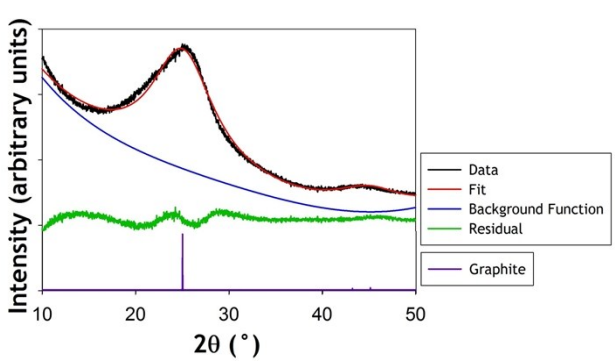

Fig. S13 The Rietveld fit (—) of the PXRD data for carbon nanofoam paper (CNF) (*i*) using a model of a graphite crystal structure.

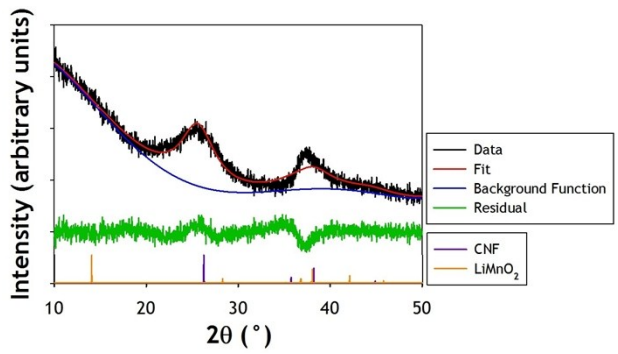

Fig. S14 The Rietveld fit (—) of the PXRD data for NaMnOx@CNF composite (ii) using a model of a graphite crystal structure; the Bragg peaks and peak intensities for birnessite $LiMnO_2$ are shown for comparison.

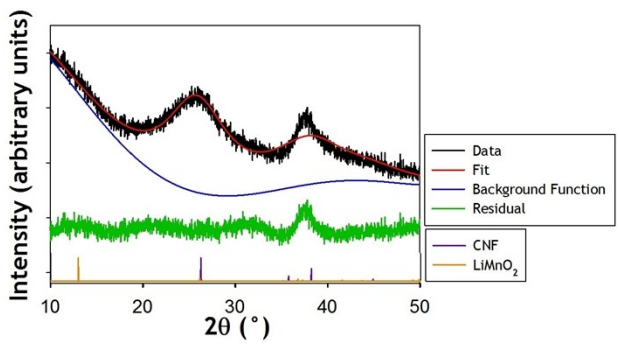

Fig. S15 The Rietveld fit (—) of the PXRD data for LiMnOx[8]@CNF composite (iii) using a model of a graphite crystal structure; the Bragg peaks and peak intensities for birnessite $LiMnO_2$ are shown for comparison.

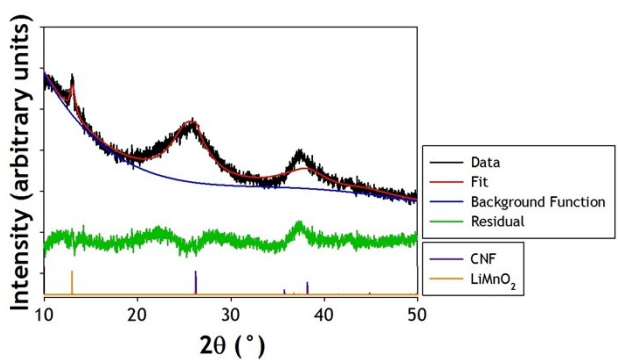

Fig. S16 The Rietveld fit (—) of the PXRD data for LiMnOx[24]@CNF composite (iv) using a model of a graphite crystal structure and a model of birnessite $LiMnO_2$.

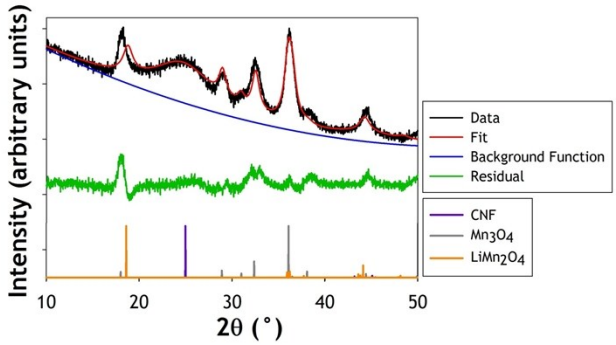

Fig. S17 The Rietveld fit (—) of the PXRD data for LiMnOx[Ar/1.33]@CNF composite (v) with graphite, tetragonal Mn_3O_4, and cubic $LiMn_2O_4$ models.

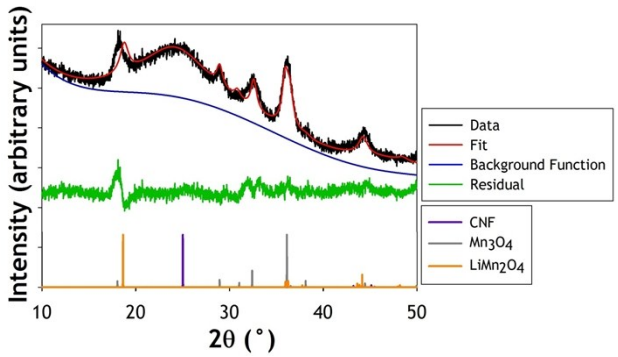

Fig. S18 The Rietveld fit (—) of the PXRD data for LiMnOx[Ar/4]@CNF composite (vi) with graphite, tetragonal Mn_3O_4, and cubic $LiMn_2O_4$ models.

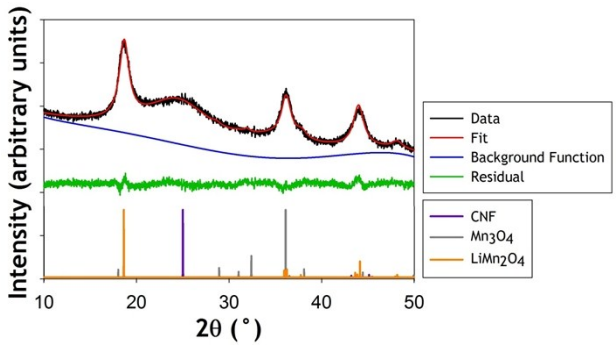

Fig. S19 The Rietveld fit (—) of the PXRD data for LiMnOx[Ar/4][Air/2]@CNF composite (vii) with graphite, tetragonal Mn_3O_4, and cubic $LiMn_2O_4$ models.

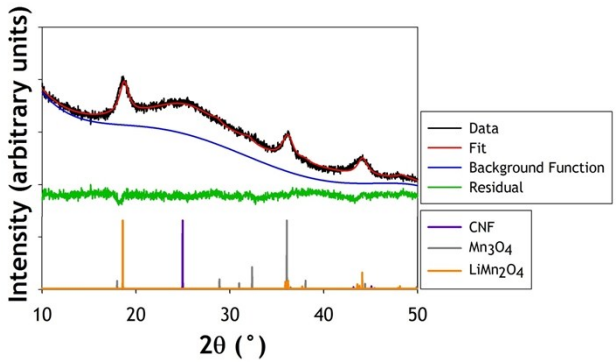

Fig. S20 The Rietveld fit (—) of the PXRD data for LiMnOx[Ar/4][Air/6]@CNF composite (*viii*) with graphite, tetragonal Mn_3O_4, and cubic $LiMn_2O_4$ models.

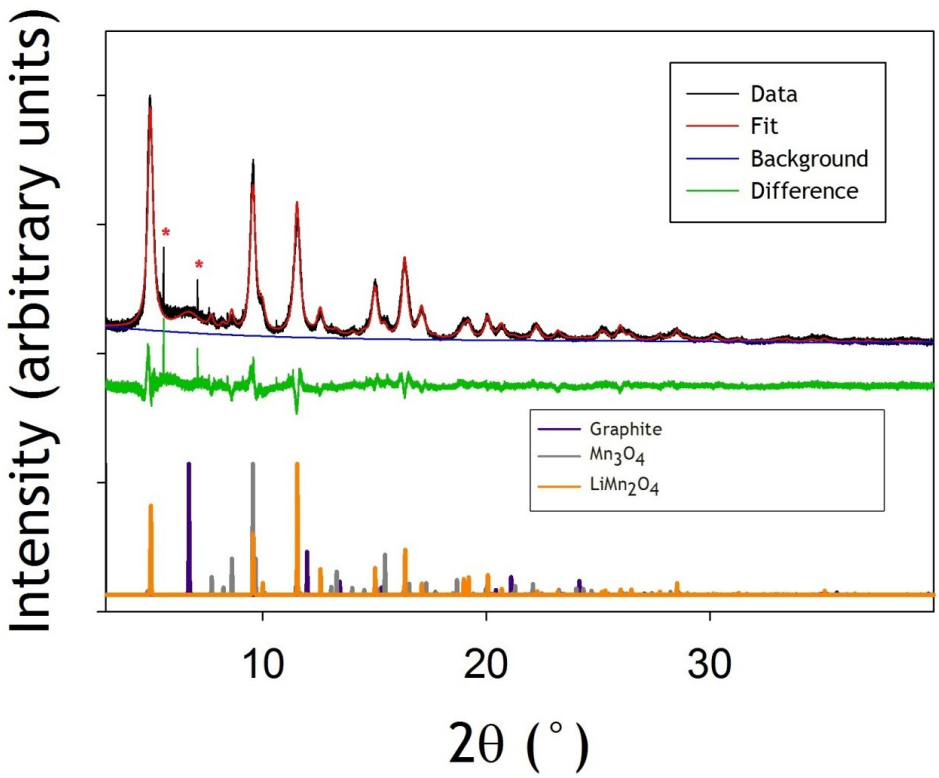

Fig. S21 The Rietveld fit (—) of composite (*viii*), LiMnOx[Ar/4][Air/6]@CNF of the PXRD data obtained at the Advanced Photon Source (λ = 0.414208 Å). An unidentified impurity exists with peaks marked with asterisks at 2θ = 5.78 and 7.10°.

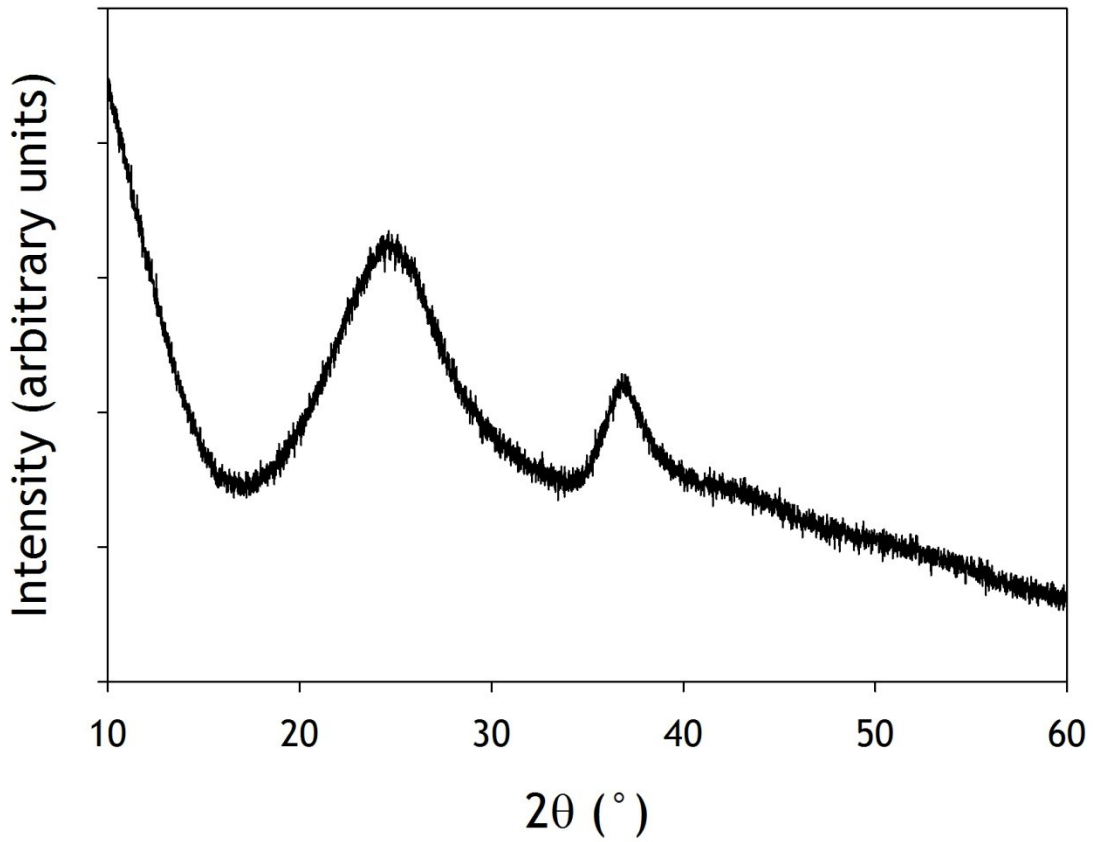

Fig. S22 The PXRD of a sample of NaMnOx@CNF after being soaked in an aqueous 1 M $NaNO_3$ solution for 24 h. No Bragg peak is observed at $2\theta \approx 13^\circ$, which indicates that no lamellar (crystalline) registry is induced by prolonged exposure to hydrated Na^+ ions while lamellar registry is achieved with prolonged exposure to a $LiNO_3$ solution (see main text).

Scanning Electron Microscopy

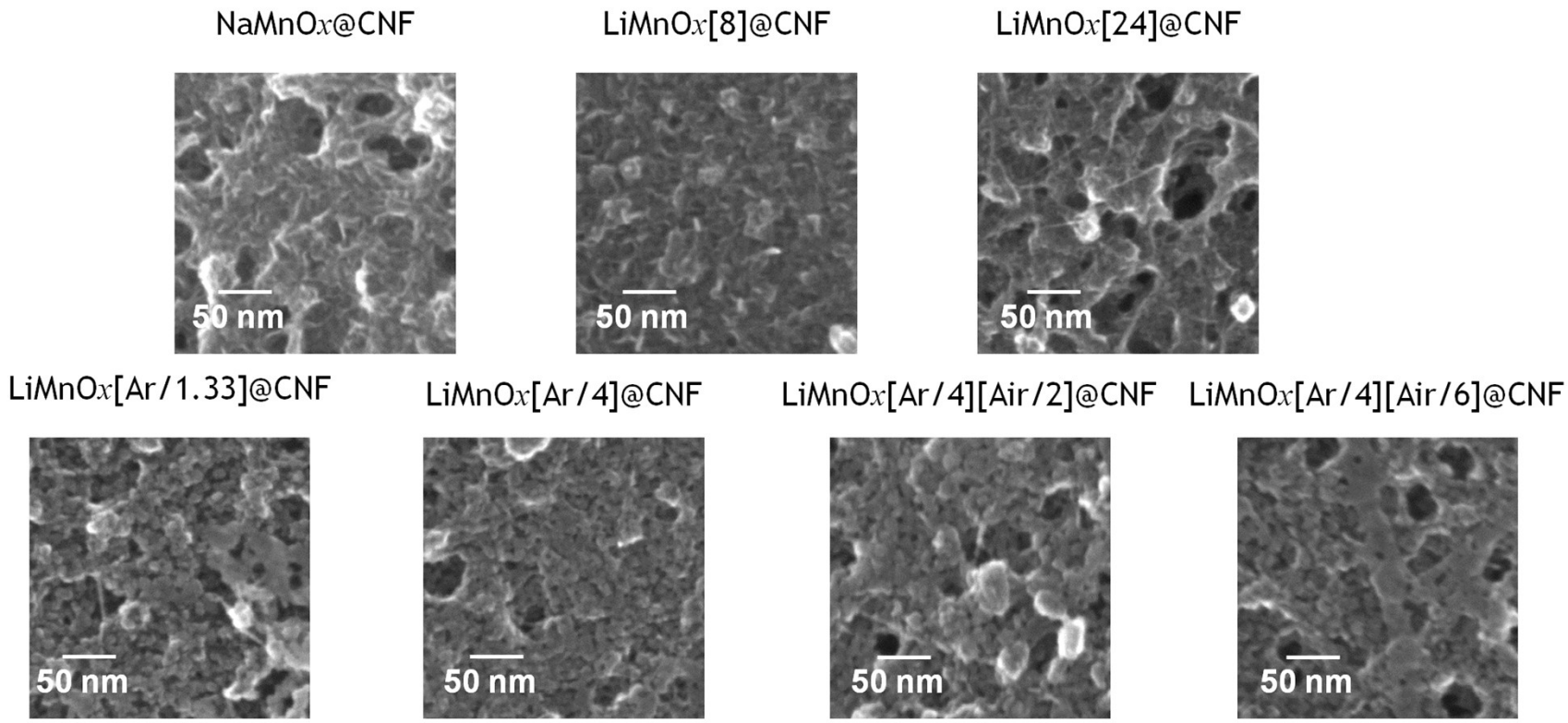

Fig. S23 Scanning electron micrographs of the MnOx@CNFs.

Pair Distribution Function (PDF) and Differential PDF (DPDF) Fits

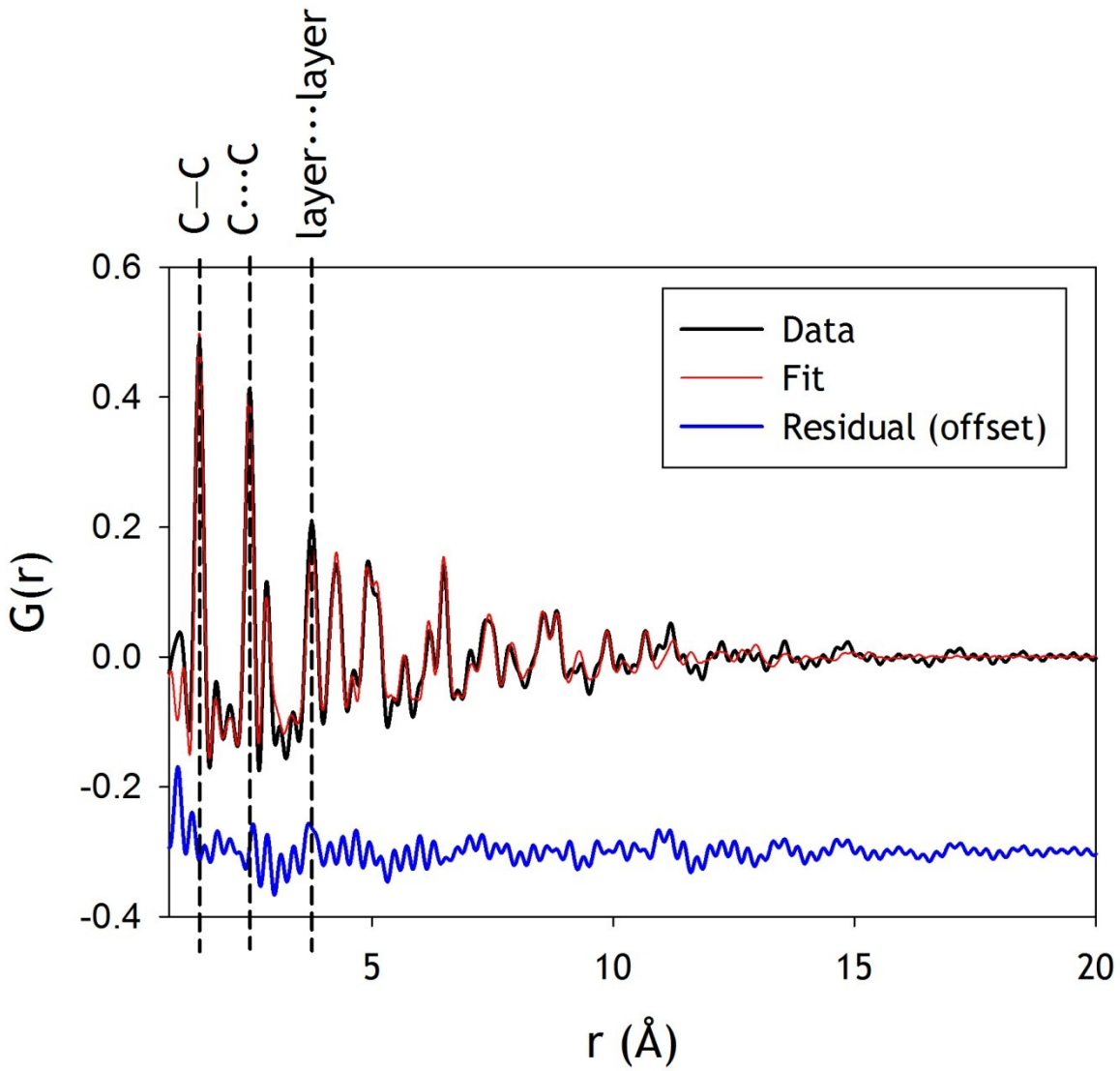

Fig. S24 The fit of the PDF data for CNF (*i*) to a model of defective graphite. The C–C bond, the first C···C interaction, and the graphite layer···layer correlations are shown.

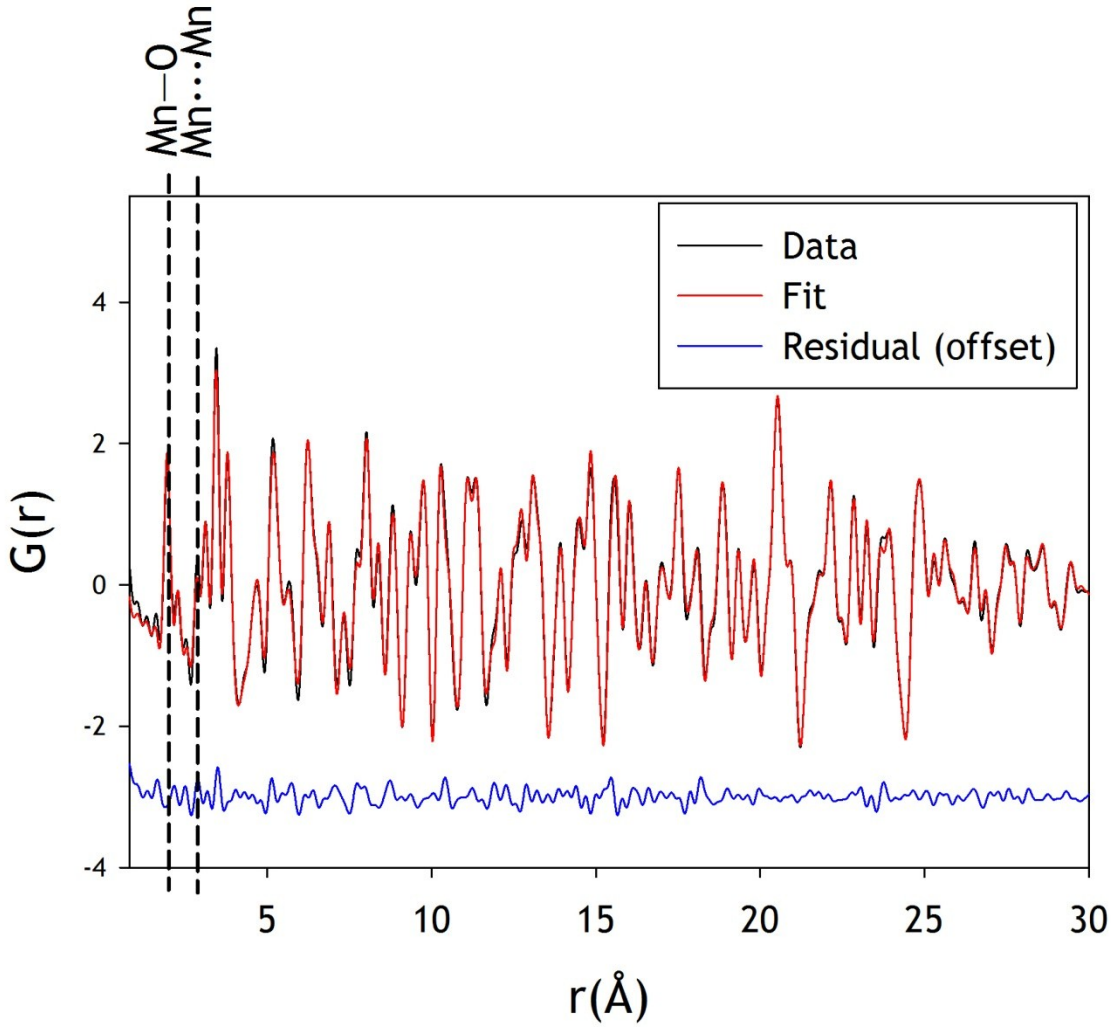

Fig. S25 The fit of the DPDF data for a 50:50 mixture (by weight) of nanoparticulate crystalline Mn_3O_4 & pulverized CNF modeled to the tetragonal hausmannite Mn_3O_4 structure. The Mn—O and the first Mn···Mn correlations are indicated.

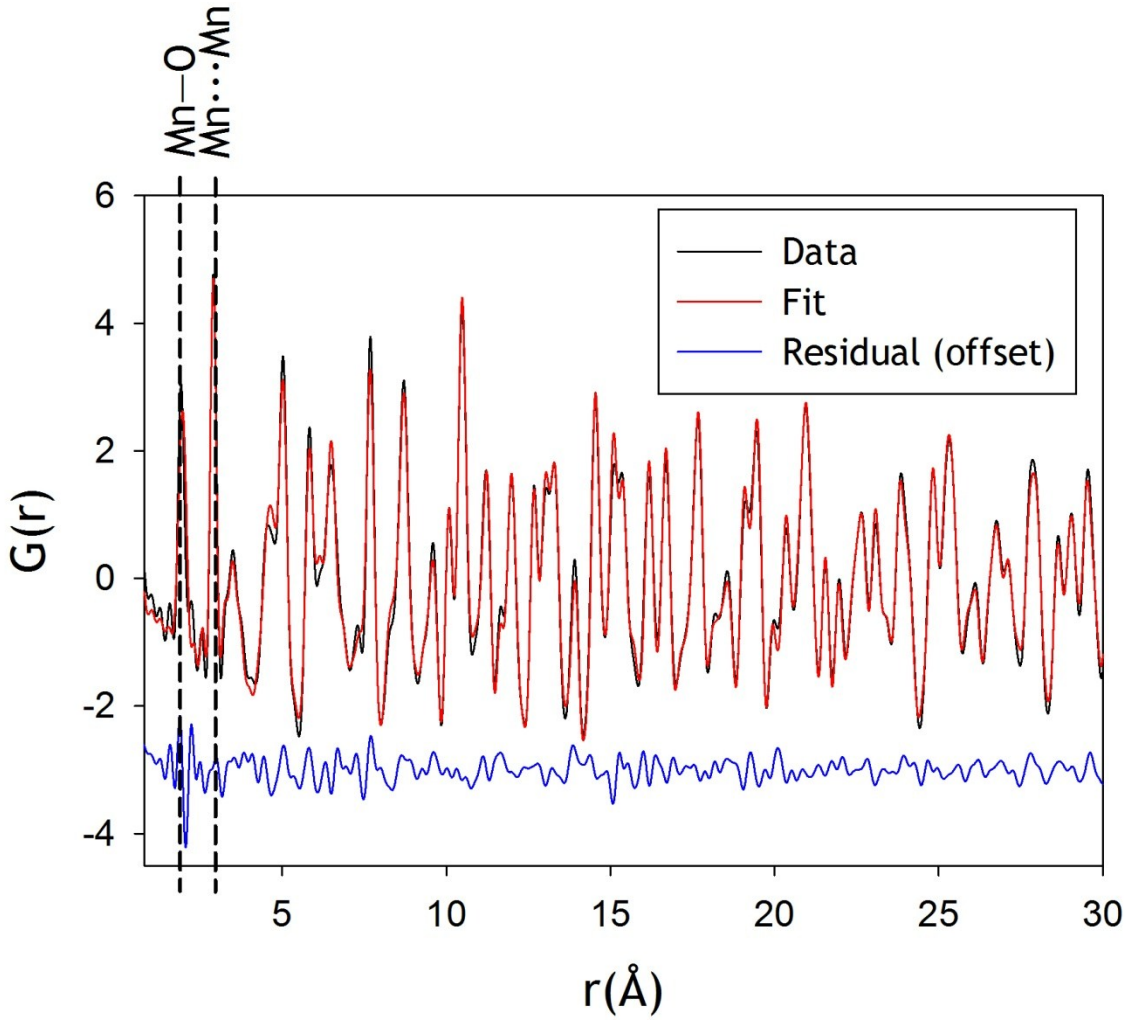

Fig. S26 The fit of the DPDF data for a 50:50 mixture (by weight) of nanocrystalline $LiMn_2O_4$ particles & pulverized CNF modeled to the cubic spinel $LiMn_2O_4$ structure. The Mn—O and the first Mn···Mn correlations are indicated.

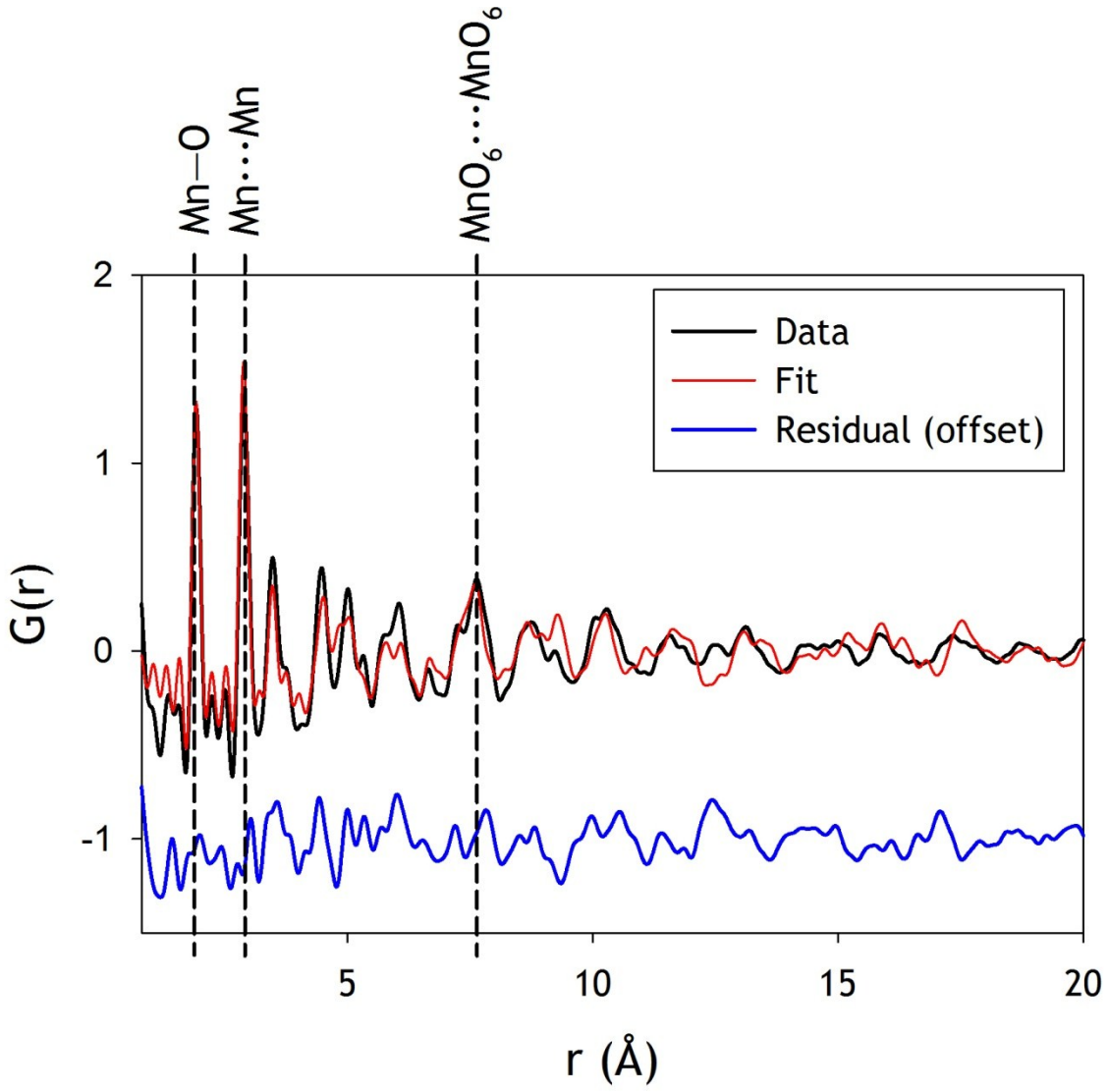

Fig. S27 The fit of the DPDF data for NaMnOx@CNF composite (ii) to a model of the birnessite structure. The Mn—O, the first Mn Mn, and $MnO_6 \cdots MnO_6$ layer interactions are indicated.

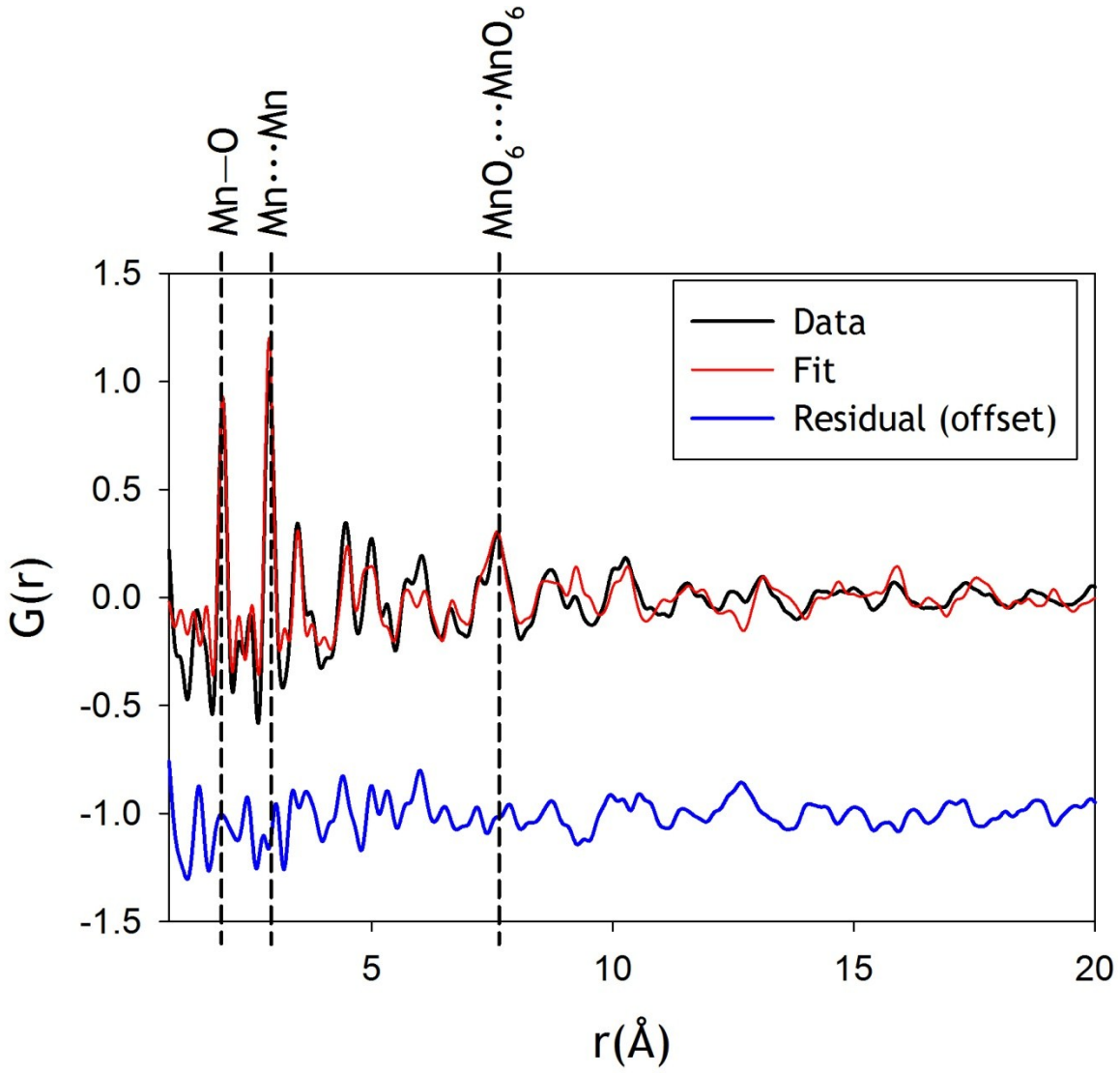

Fig. S28 The fit of the DPDF data for LiMnOx[8]@CNF composite (*iii*) to a model of the birnessite structure. The Mn–O, the first Mn Mn, and $MnO_6 \cdots MnO_6$ layer interactions are indicated.

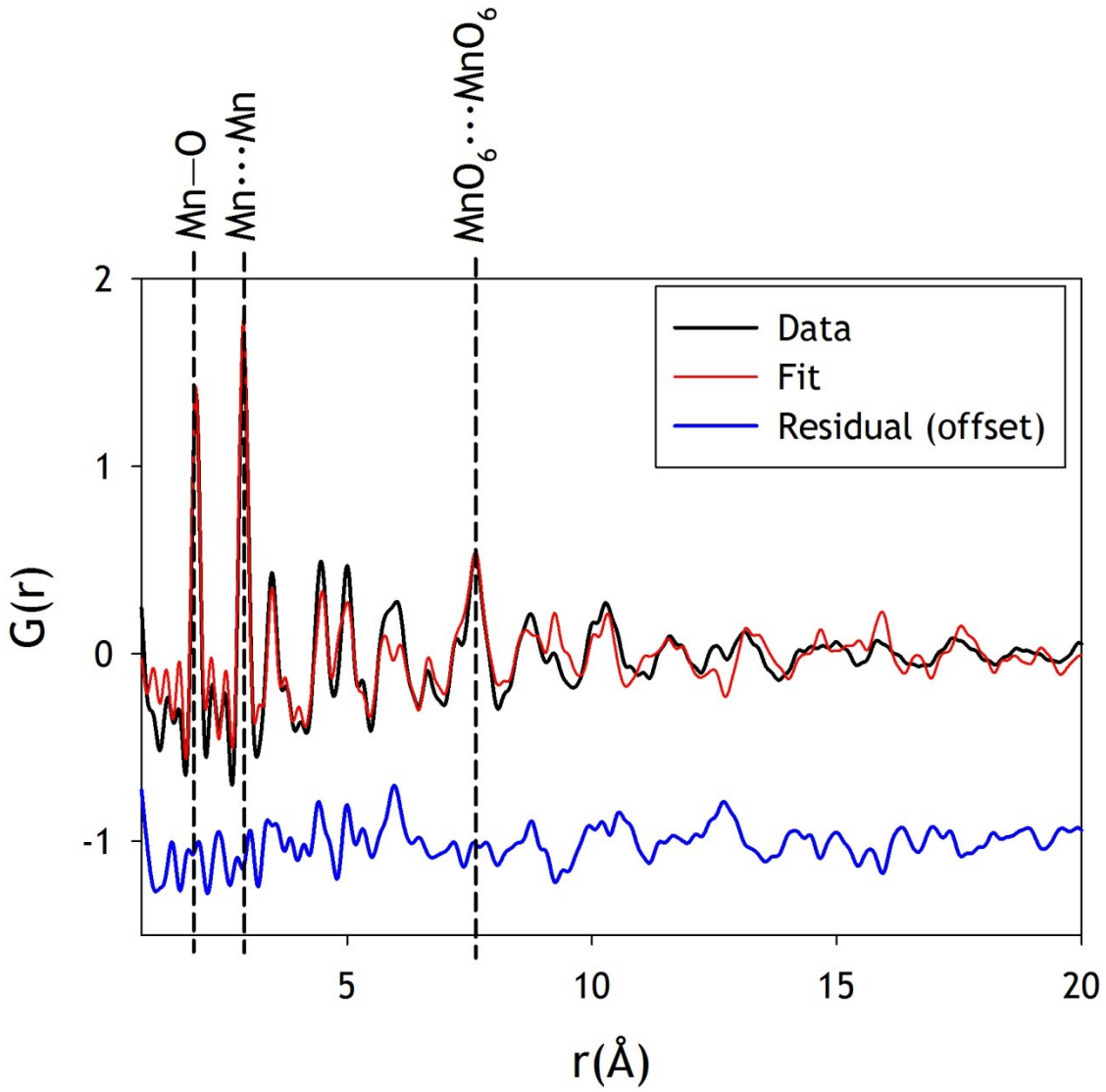

Fig. S29 The fit of the DPDF data for LiMnOx[24]@CNF composite (iv) to a model of the birnessite structure. The Mn–O, the first Mn Mn, and MnO_6···MnO_6 layer interactions are indicated.

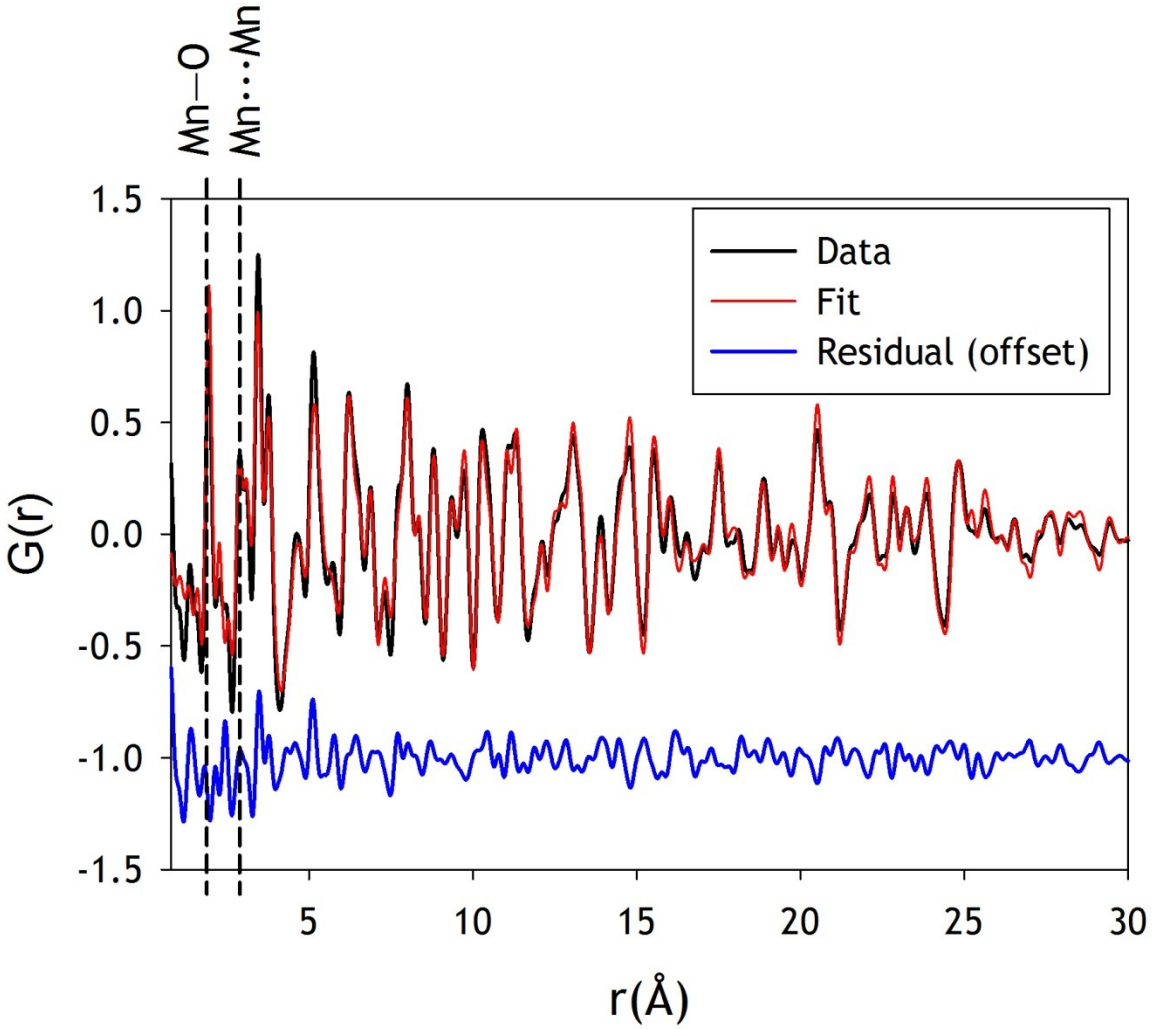

Fig. S30 The fit of the DPDF data for LiMnOx[Ar/1.33]@CNF composite (v) to a combination of birnessite, cubic spinel $LiMn_2O_4$, and tetragonal hausmannite Mn_3O_4 structural models.

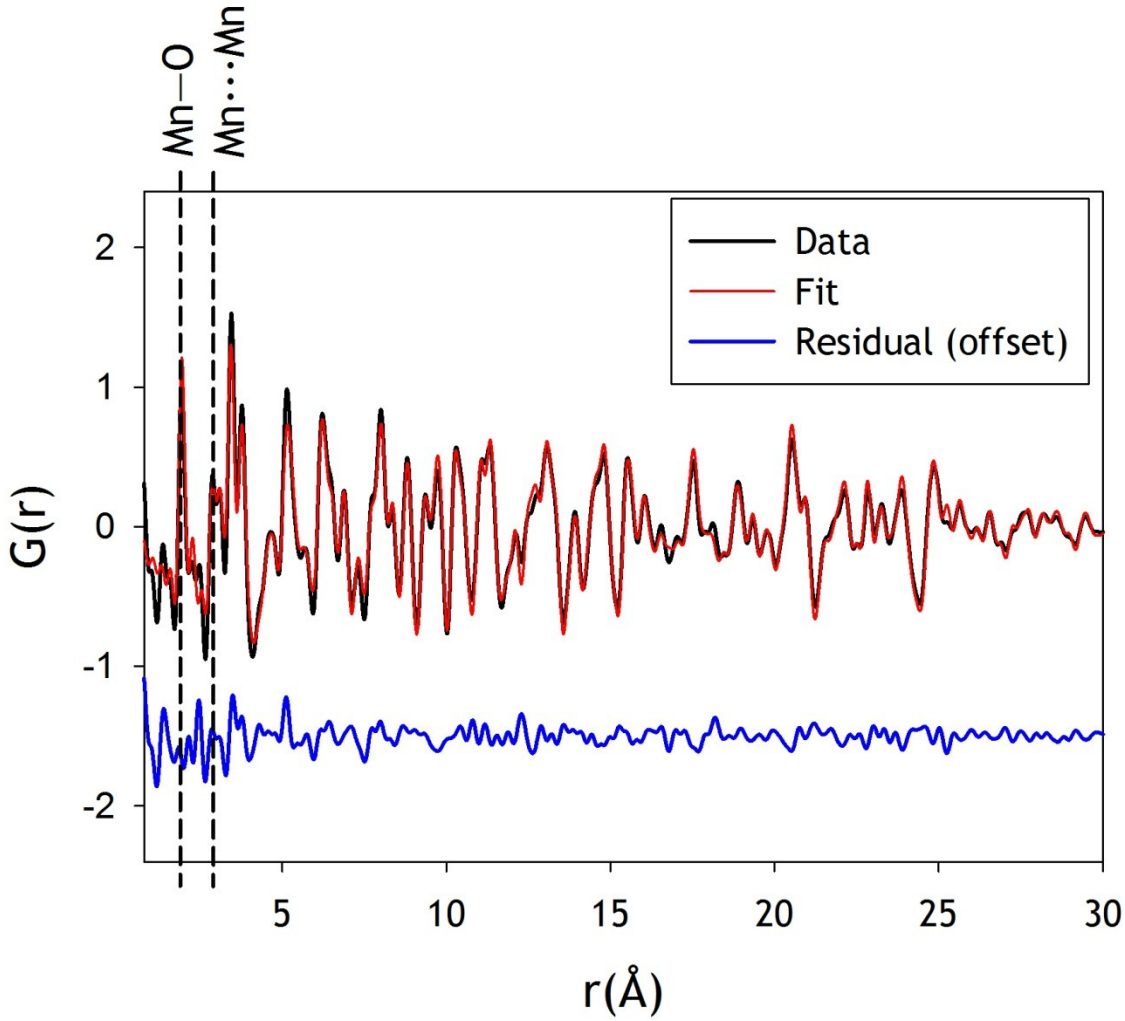

Fig. S31 The fit of the DPDF data for LiMnOx[Ar/4]@CNF composite (vi) to a combination of birnessite, cubic spinel $LiMn_2O_4$, and tetragonal hausmannite Mn_3O_4 structural models.

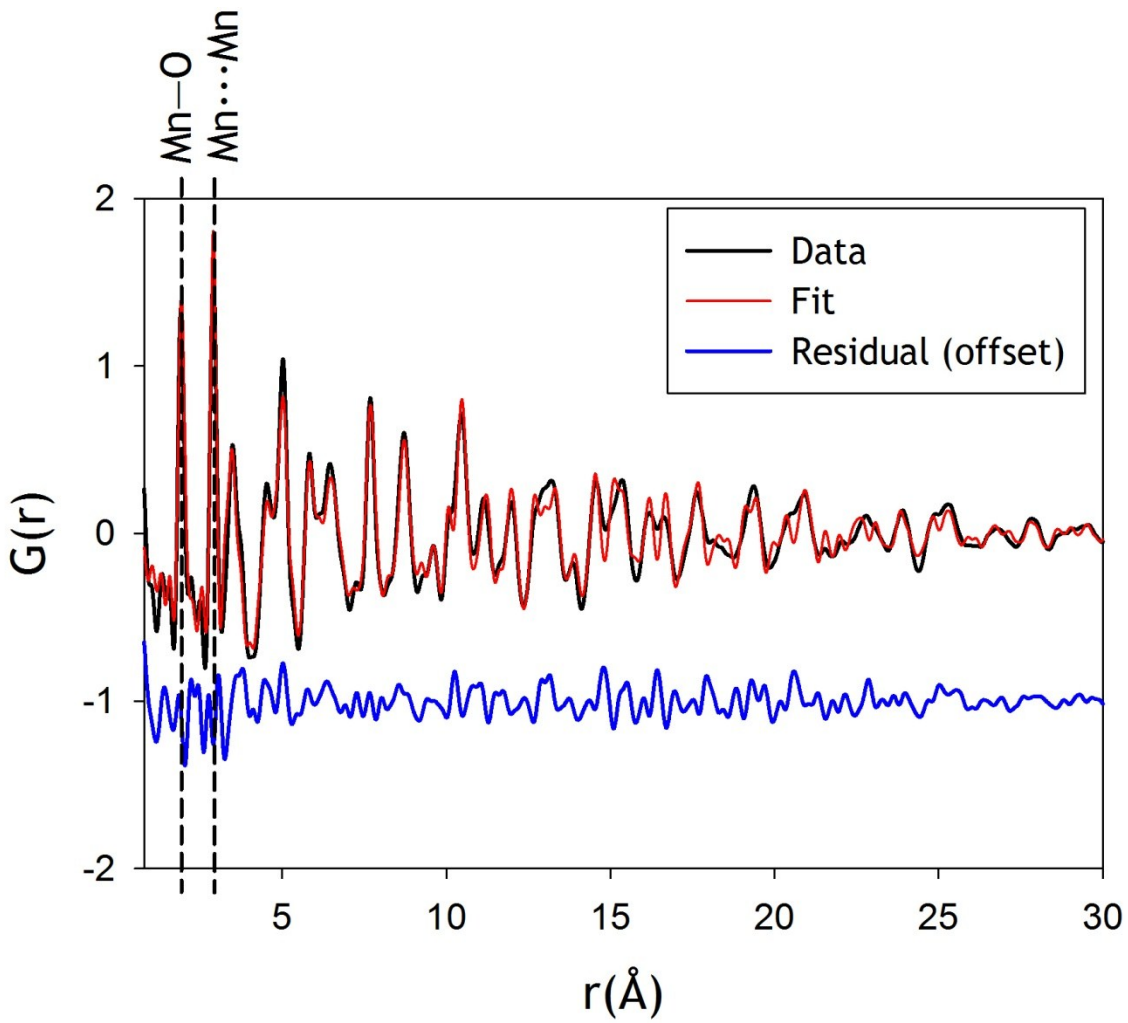

Fig. S32 The fit of the DPDF data for LiMnOx[Ar/4][Air/2] composite (*vii*) to a combination of birnessite, cubic spinel $LiMn_2O_4$, and tetragonal hausmannite Mn_3O_4 structural models.

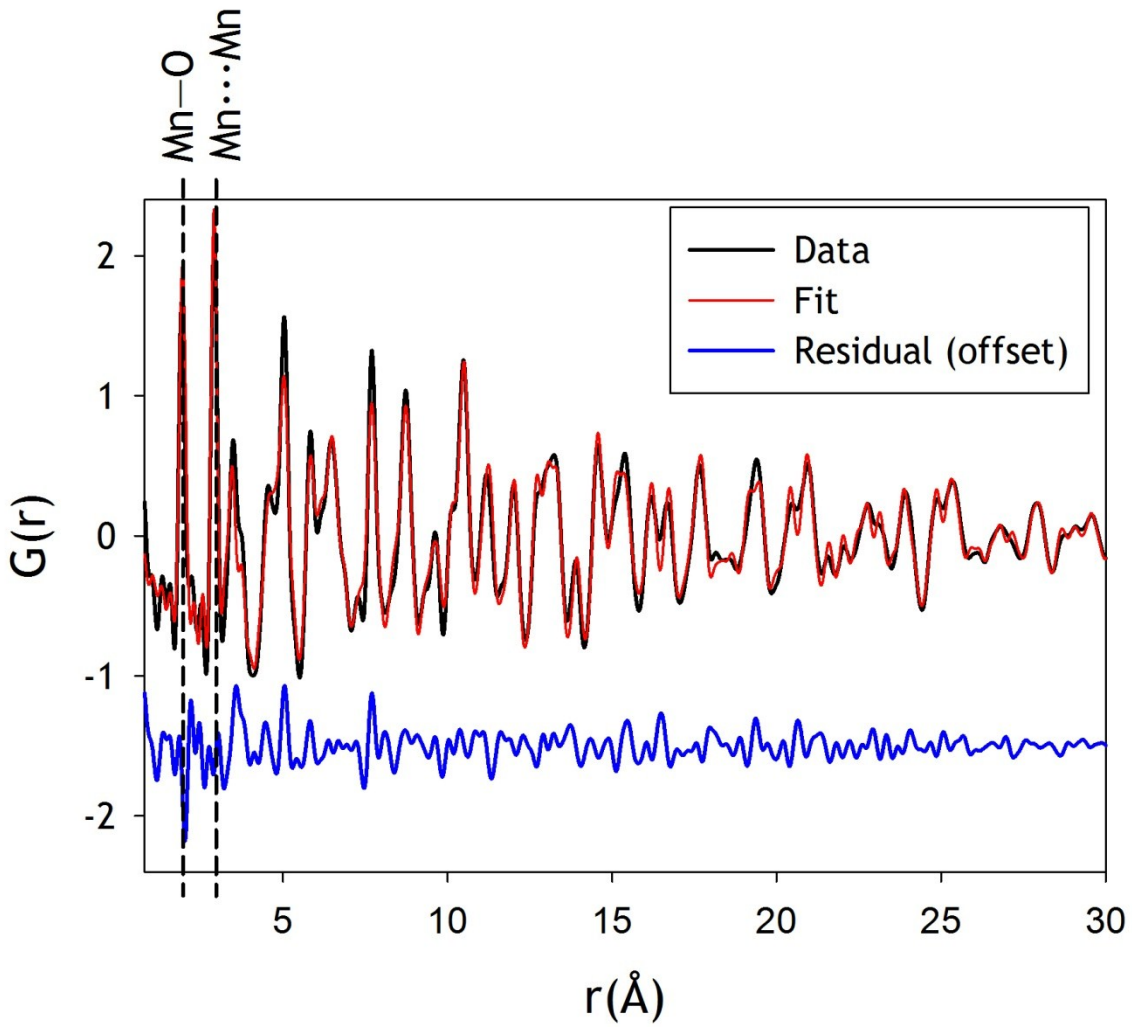

Fig. S33 The fit of the DPDF data for LiMnOx[Ar/4][Air/6] composite (*viii*) to a combination of birnessite, cubic spinel $LiMn_2O_4$, and tetragonal hausmannite Mn_3O_4 structural models.

DPDFs with Varied Scale Factors

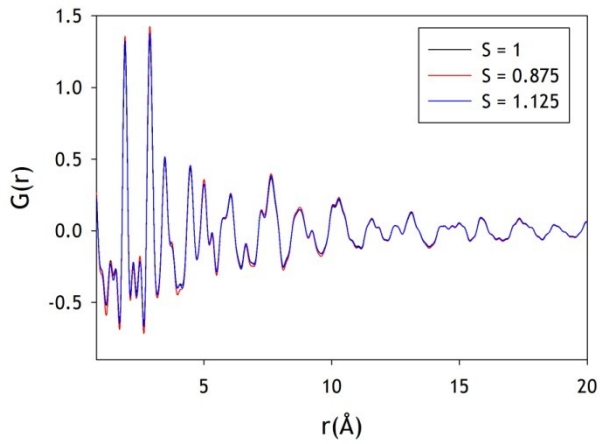

Fig. S34 The DPDFs for NaMnOx@CNF composite (*ii*) generated with a scale factor (S) of 1 ± 12.5%: little to no variance is observed.

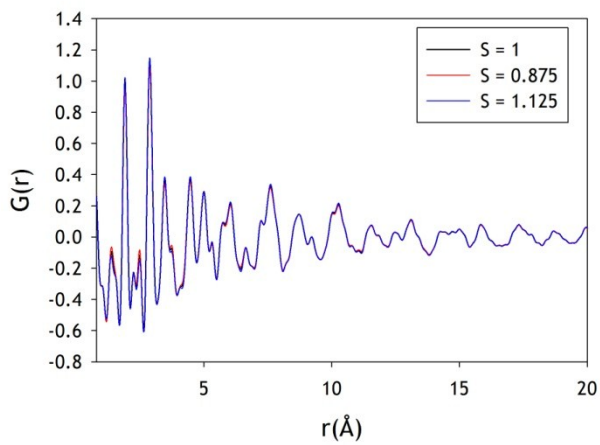

Fig. S35 The DPDFs for LiMnOx[8]@CNF composite (*iii*) generated with a scale factor (S) of 1 ± 12.5%: little to no variance is observed.

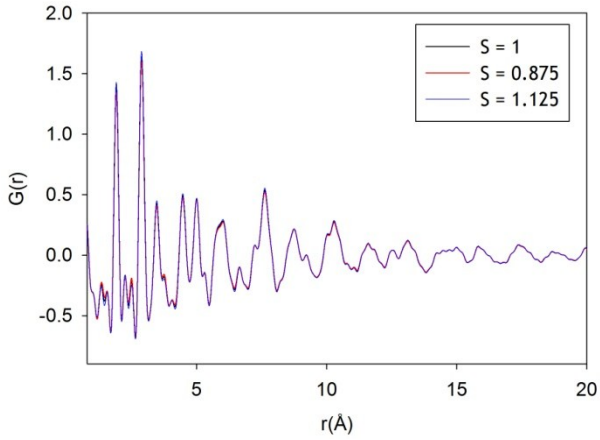

Fig. S36 The DPDFs for LiMnOx[24]@CNF composite (iv) generated with a scale factor (S) of 1 ± 12.5%: little to no variance is observed.

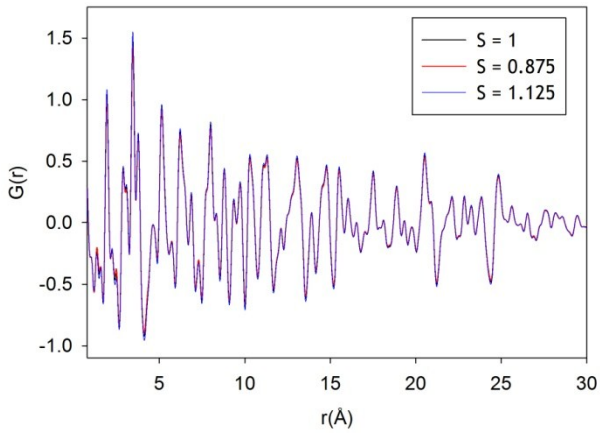

Fig. S37 The DPDFs for LiMnOx[Ar/1.33]@CNF composite (v) generated with a scale factor (S) of 1 ± 12.5%: little to no variance is observed.

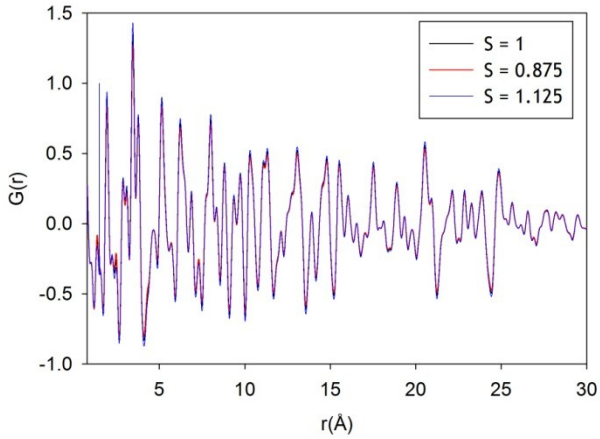

Fig. S38 The DPDFs for LiMnOx[Ar/4]@CNF composite (vi) generated with a scale factor (S) of 1 ± 12.5%: little to no variance is observed.

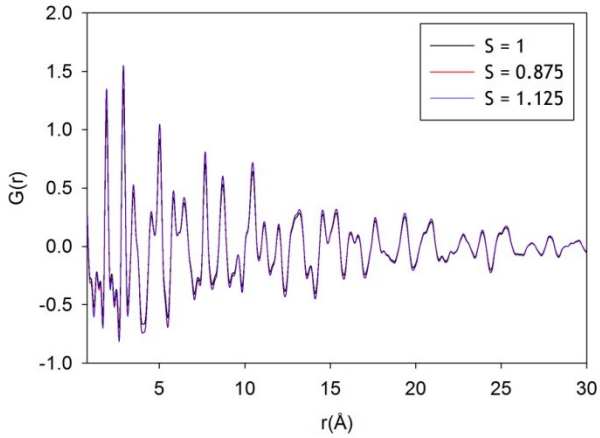

Fig. S39 The DPDFs for LiMnOx[Ar/4][Air/2]@CNF composite (vii) generated with a scale factor (S) of 1 ± 12.5%: little to no variance is observed.

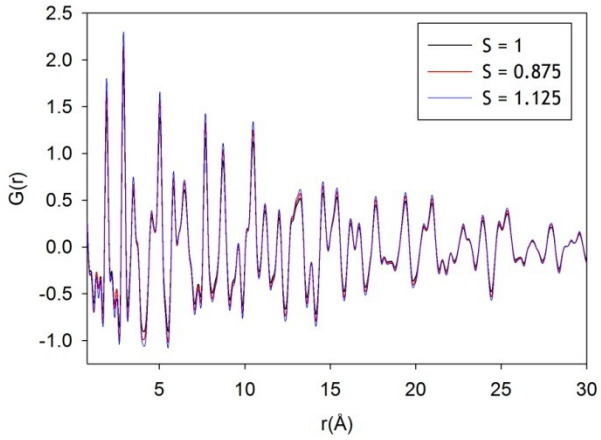

Fig. S40 The DPDFs for LiMnOx[Ar/4][Air/6]@CNF composite (*viii*) generated with a scale factor (S) of 1 ± 12.5%: little to no variance is observed.

Fit parameters for the PXRD, PDF, and DPDF Data

Table S2 The fit parameters for the DPDF analysis of Mn_3O_4 & CNF mixture (50:50 by weight)

Material:	Mn_3O_4 & CNF Mixture	
Phase	**DPDF Analysis**	
	Scale Factor	0.389
Tetragonal Mn_3O_4	a (Å)	5.75426
	b (Å)	5.75426
	c (Å)	9.45708
	Fitness	R_w = 0.108

Table S3 The fit parameters for the DPDF analysis of $LiMn_2O_4$ & CNF mixture (50:50 by weight)

Material:	$LiMn_2O_4$ & CNF Mixture	
Phase	**DPDF Analysis**	
	Scale Factor	0.425
Cubic $LiMn_2O_4$	a (Å)	8.22031
	b (Å)	8.22031
	c (Å)	8.22031
	Fitness	R_w = 0.141

Table S4 The fit parameters for the PXRD and DPDF data for CNF (*i*)

Material:	(*i*) CNF			**Atom Distances from DPDF analyses**	
Phase	**PXRD analysis**		**DPDF analysis**		
Graphite	Parameter	Refined Values	Refined Values		
	a (Å)	2.416115	2.452928	C–C	1.4206
	b (Å)	2.416115	2.452928	C···C intralayer	3.6774
	c (Å)	7.116933	7.354822		
	Occupancy* C2	—	0.356		
	Turbostratic disorder term†	—	137		
	Size (nm)	1.12	1.85		
	Fitness	wR = 3.676%	R_w = 0.252		

* The occupancy of the carbon atoms located at (0, 0, 0) and ($^1/_3$, $^2/_3$, 0) was refined. The carbon at (0, 0, 0) refined to ~1, but the carbon atom located at ($^1/_3$, $^2/_3$, 0) deviated from 1 significantly and was refined. This large deviation may not be quantifiably accurate as the model supposes a semicrystalline graphitic model rather than a truly amorphous model.

† The turbostratic disorder term was defined by one variable (unitless) that is multiplied to the displacement parameters of all atoms along the *c* axis.

Table S5 The fit parameters for the PXRD and DPDF data for NaMnOx@CNF composite (ii). Contributions of the CNF were removed for DPDF analysis. The PXRD data were fit over 2θ = 10–50°; the DPDF data were fit over r = 0.8–20 Å.

Material:	(ii) NaMnOx@CNF				
Phase	**PXRD analysis**		**DPDF Analysis**		
Graphite	Parameter	Refined Values	Refined Values		
$P6_3mc$ spacegroup	a (Å)	2.896322	—		
	b (Å)	2.896322	—		
	c (Å)	6.95872	—		
	Size (nm)	1.12	—		
	R_w (fitness)	—	0.427	**Atom Distances and Number of Bonds from DPDF analyses**	
Birnessite NaMnOx	Scale Factor	—	0.155		
$C2/m$ spacegroup	a (Å)	—	5.047976	Mn–O (Å)	1.8972 × 4 2.0019 × 2
	b (Å)	—	2.866402	Na–O (Å)	3.0109 × 4 3.5171 × 2
	c (Å)	—	7.862134	Na···Na‡ (Å)	2.8664
	β (°)	—	113.211	Mn···Mn‡ (Å)	2.8664
	Turbostratic disorder term	—	56.2*	O···O‡ (Å)	2.4863
	Particle Size (nm)	—	4†		
	Na^+ occupancy:	—	0.864		
	Fitness	wR = 2.437%	R_w = 0.427		

*The turbostratic disorder term was defined by one variable (unitless) that is multiplied to the thermal displacement parameters of all atoms along the *c* axis.

† Size fixed to account for correlations at r = 20–30 Å

‡ First A···A correlation

Table S6 The fit parameters for the PXRD and DPDF data for LiMnOx[8]@CNF composite (*iii*). Contributions of the CNF were removed for DPDF analysis. The PXRD data were fit over 2θ = 10–50°; the DPDF data were fit over r = 0.8–20 Å.

Material:	(*iii*) LiMnOx[8]@CNF				
Phase	**PXRD analysis**		**DPDF Analysis**		
Graphite	Parameter	Refined Values	Refined Values		
$P6_3mc$ spacegroup	a (Å)	2.88181	—		
	b (Å)	2.88181	—		
	c (Å)	6.898756	—		
	Size (nm)	1.00	—		
Birnessite LiMnOx	Scale Factor	—	0.0739	**Atom Distances and Number of Bonds from DPDF analyses**	
$C2/m$ spacegroup	a (Å)	—	5.05543		
	b (Å)	—	2.85260	Mn–O (Å)	1.8952 × 4 1.9603 × 2
	c (Å)	—	7.52340	Li–O (Å)	2.9633 × 4 3.3476 × 2
	β (°)	—	110.774	Li···Li¶ (Å)	2.8526
	Turbostratic disorder term†	—	53.5*	Mn···Mn¶ (Å)	2.8526
	Particle Size (nm)	—	4†	O···O¶ (Å)	2.4959
	Li^+ occupancy:	—	2.69‡		
	Fitness	wR = 3.026%	R_w = 0.441		

***** The turbostratic disorder term was defined by one variable (unitless) that is multiplied to the displacement parameters of all atoms along the *c* axis.

† Size fixed to account for correlations at r = 20–30 Å.

‡ 'Over occupancy likely occurs on account of presence of sodium ions and/or water molecules at Li^+ sites.

¶ First A···A correlation

Table S7 The fit parameters for the PXRD and DPDF data for LiMnOx[24]@CNF composite (iv). Contributions of the CNF were removed for DPDF analysis. The PXRD data were fit over 2θ = 10–50°; the DPDF data were fit over r = 0.8–20 Å.

Material:	(iv) LiMnOx[24]@CNF				
Phase	**PXRD Analysis**		**DPDF Analysis**		
Graphite	Parameter	Refined Values	Refined Values		
$P6_3mc$ spacegroup	a (Å)	2.88772	—		
	b (Å)	2.88772	—		
	c (Å)	6.97411	—		
	Size (nm)	1.92	—		
LiMnOx birnessite	Scale Factor	—	0.119	**Atom Distances and Number of Bonds from DPDF analyses**	
$C2/m$ spacegroup	a (Å)	5.10862*	5.06831		
	b (Å)	2.85194*	2.85809	Mn–O (Å)	1.9005 × 4 2.0507 × 2
	c (Å)	7.349286*	7.45818	Li–O (Å)	2.8986 × 4 3.2322 × 2
	β (°)	111.81*	110.839	Li···Li¶ (Å)	2.8519
	Turbostratic disorder term†	—	44.6	Mn···Mn¶ (Å)	2.8919
	Size (nm)	1.00*	4‡	O···O¶ (Å)	2.5057
	Li^+ site 'occupancy'	—	2.28§		
	Fitness	wR = 2.409%	R_w = 0.377		

* The values are unreliable because of an insufficient number of peaks for suitable refinement.

† The turbostratic disorder term was defined by one variable (unitless) that is multiplied to the displacement parameters of all atoms along the *c* axis.

‡ Fixed to account for correlations between 20–30 Å.

§ 'Over occupancy likely occurs on account of presence of sodium ions and/or water molecules at Li^+ sites.

¶ First A···A correlation.

Table S8 The fit parameters for the PXRD and DPDF data for LiMnOx[Ar/1.33]@CNF composite (v). Contributions of the CNF were removed for DPDF analysis. The PXRD data were fit over 2θ = 10–50°; The DPDF data were fit over r = 0.8–30 Å.

Material:	(v) LiMnOx[Ar/1.33]@CNF				
Phase	**PXRD Analysis**		**DPDF Analysis**		
Graphite	Parameter	Refined Values	Refined Values		
$P6_3mc$ spacegroup	a (Å)	2.88760	—		
	b (Å)	2.88760	—		
	c (Å)	7.21308	—		
	Size (nm)	1.33	—		
LiMnOx[24] structure	Scale Factor	—	0.0117*	**Atom Distances and Number of Bonds from DPDF analyses**	
Cubic $LiMn_2O_4$	Scale Factor	—	0.119		
	a (Å)	8.18526	8.38647	Li–O (Å)	1.9834 × 4
	b (Å)	8.18526	8.38647	Mn–O (Å)	1.9682 × 6
	c (Å)	8.18526	8.38647	Mn···Mn‡ (Å)	2.9296
	Size (nm)	7.08	10†		
	Scale Factor	—	0.156		
Tetragonal Mn_3O_4	a (Å)	5.78066	5.76257	Mn_{Td}–O (Å)	1.8601 × 4
	b (Å)	5.78066	5.76257	Mn_{Oh}–O (Å)	2.0371 × 4 2.3537 × 2
	c (Å)	9.38832	9.41299	Mn···Mn‡ (Å)	2.8809
	Size (nm)	10.15	10†		
	Fitness	wR = 3.908%	R_w = 0.262		

***** The structure of LiMnOx[24] in composite (iv) was used; the scale factor was the only value refined in order to minimize variables.

† The particle size was fixed based upon estimates from the PXRD data.

‡ First Mn···Mn correlation.

Table S9 The fit parameters for the PXRD and DPDF data for LiMnOx[Ar/4]@CNF composite (*vi*). Contributions of the CNF were removed for DPDF analysis. The PXRD data were fit over 2θ = 10–50°; DPDF was fit over r = 0.8–30 Å.

Material:	(vi) LiMnOx[Ar/4]@CNF				
Phase	**PXRD Analysis**		**DPDF Analysis**		
Graphite	Parameter	Refined Values	Refined Values		
$P6_3mc$ spacegroup	a (Å)	2.42574	—		
	b (Å)	2.42574	—		
	c (Å)	7.16120	—		
	Size (nm)	1.00	—		
LiMnOx[24] structure	Scale Factor	—	0.00852*	**Atom Distances and Number of Bonds from DPDF analyses**	
Cubic $LiMn_2O_4$	Scale Factor	—	0.0157*	Li–O (Å)	1.9685 × 4
$Fm\bar{3}m$ spacegroup	a (Å)	8.20178	8.22352	Mn–O (Å)	1.9534 × 6
	b (Å)	8.20178	8.22352	Mn···Mn‡ (Å)	2.9075
	c (Å)	8.20178	8.22352		
	Size (nm)	8.86	10†		
Tetragonal Mn_3O_4	Scale Factor	—	0.197	Mn_{Td}–O (Å)	1.8616 × 4
$I4_1/amd$ spacegroup	a (Å)	5.79278	5.7664	Mn_{Oh}–O (Å)	2.0387 × 4 2.3557 × 2
	b (Å)	5.79278	5.7664	Mn···Mn‡ (Å)	2.8832
	c (Å)	9.35263	9.42285		
	Size (nm)	6.91	10†		
	Fitness	wR = 3.149%	R_w = 0.223		

* The structure of LiMnOx[24] in composite (*iv*) was used; the scale factor was the only value refined in order to minimize variables.

† The particle size was fixed based upon estimates from the PXRD data.

‡ First Mn···Mn correlation.

Table S10 The fit parameters for the PXRD and DPDF data for LiMnOx[Ar/4][Air/2]@CNF (vii). Contributions of the CNF were removed for DPDF analysis. The PXRD data were fit over 2θ = 10–50°; the DPDF data were fit over r = 0.8–30 Å.

Material:	(vii) LiMnOx[Ar/4][Air/2]@CNF				
Phase	**PXRD Analysis**		**DPDF Analysis**		
Graphite	Parameter	Refined Values			
P6₃mc spacegroup	a (Å)	3.12846	—		
	b (Å)	3.12846	—		
	c (Å)	7.28179	—		
	Size (nm)	1.01			
LiMnOx[24] structure	Scale Factor	—	0.00852*	**Atom Distances and Number of Bonds from DPDF analyses**	
Cubic $LiMn_2O_4$	Scale Factor	—	0.136	Li–O (Å)	1.9668 × 4
$Fm\bar{3}m$ spacegroup	a (Å)	8.23189	8.21672	Mn–O (Å)	1.9518 × 6
	b (Å)	8.23189	8.21672	Mn···Mn‡ (Å)	2.9050
	c (Å)	8.23189	8.21672		
	Size (nm)	7.25	4.666		
Tetragonal Mn_3O_4	Scale Factor	—	0.0580	Mn_{Td}–O (Å)	1.8255 × 4
$I4_1/amd$ spacegroup	a (Å)	5.77536	5.7048	Mn_{Oh}–O (Å)	2.0170 × 4 2.2789 × 2
	b (Å)	5.77536	5.7048	Mn···Mn‡ (Å)	2.8524
	c (Å)	9.62657	9.1154		
	Size (nm)	10.78	2.548		
	Fitness	wR = 2.106%	R_w =0.263		

*The structure of LiMnOx[24] in composite (iv) was used; the scale factor was the only value refined in order to minimize variables.

† First Mn···Mn correlation.

Table S11 The fit parameters for the PXRD data for LiMnOx[Ar/4][Air/6]@CNF ($viii$); the data were fit over 2θ = 10–50°.

Material:	($viii$) LiMnOx[Ar/4][Air/6]@CNF	
Phase	**PXRD Analysis**	
Graphite	Parameter	Refined Values
$P6_3mc$ spacegroup	a (Å)	2.95265
	b (Å)	2.95265
	c (Å)	7.25612
	Size (nm)	1.00
Cubic $LiMn_2O_4$	a (Å)	8.20975
$Fm\bar{3}m$ spacegroup	b (Å)	8.20975
	c (Å)	8.20975
	Size (nm)	7.66
Tetragonal Mn_3O_4	a (Å)	5.80091
$I4_1/amd$ spacegroup	b (Å)	5.80091
	c (Å)	9.59207
	Size (nm)	7.53
	Fitness	wR = 2.949%

Table S12 The fit parameters for synchrotron radiation PXRD and DPDF data for LiMnOx[Ar/4][Air/6]@CNF composite (*viii*). Contributions of the CNF were removed for DPDF analysis. The PXRD data were fit over 2θ = 10–50°; the DPDF data were fit over r = 0.8–30 Å.

Material:	(*viii*) LiMnOx[Ar/4][Air/6]@CNF				
Phase	**PXRD Analysis**		**DPDF Analysis**		
Graphite	Parameter	Refined Values			
$P6_3mc$ spacegroup	a (Å)	2.38729	—		
	b (Å)	2.38729	—		
	c (Å)	7.08216	—		
	Size (nm)	1.8	—		
LiMnOx[24] structure	Scale Factor	—	0.0123*	**Atom Distances and Number of Bonds from DPDF analyses**	
Cubic $LiMn_2O_4$	Scale Factor	—	0.207	Li–O (Å)	1.9699 × 4
	a (Å)	8.23726	8.22936	Mn–O (Å)	1.9548 × 6
	b (Å)	8.23726	8.22936	Mn···Mn‡ (Å)	2.9095
	c (Å)	8.23726	8.22936		
	Size (nm)	8.73	10.931		
Tetragonal Mn_3O_4	Scale Factor	—	0.0481	Mn_{Td}–O (Å)	1.8577 × 4
$Fm\bar{3}m$ spacegroup	a (Å)	5.76092	5.73805	Mn_{Oh}–O (Å)	2.0287 × 4 2.3606 × 2
	b (Å)	5.76092	5.73805	Mn···Mn‡ (Å)	2.8690
	c (Å)	9.40507	9.44233		
	Size (nm)	11.10	5.700		
	Fitness	wR = 9.584%	R_w = 0.247		

* The structure of LiMnOx[24] in composite (*iv*) was used; the scale factor was the only value refined in order to minimize variables.

† First correlation.

Citation

1. A. C. Ferrari and J. Robertson, Interpretation of Raman Spectra of Disordered and Amorphous Carbon, *Phys. Rev. B*, 2000, **61**, 14095–14107.

Acknowledgements

This work was supported by the U. S. Office of Naval Research. M. D. D. acknowledges the National Research Council for a Postdoctoral Fellowship (2014–2016). This research used resources of the Advanced Photon Source (APS), a U. S. Department of Energy (DOE) Office of Science User Facility operated for the DOE Office of Science by Argonne National Laboratory under Contract No. DE-AC02-06CH11357. The PDF experiments were conducted at 11-ID-B of the APS. A synchrotron PXRD pattern was obtained via the mail-in program at 11-BM of the APS. We thank Dr. Mikhail Feygenson (Oak Ridge National Laboratory) and the 11-ID-B/NOMAD partner program for initial data collection of pair distribution function data.